



PERGAMON

Micron 30 (1999) 425–436

micron

www.elsevier.com/locate/micron

Investigating the atomic scale structure and chemistry of grain boundaries in high- T_c superconductors

N.D. Browning^{a,*}, J.P. Buban^a, C. Prouteau^{a,b,1}, G. Duscher^{a,b}, S.J. Pennycook^b^a*Department of Physics (M/C 273), University of Illinois at Chicago, 845 West Taylor Street, Chicago, IL 60607-7059, USA*^b*Solid State Division, Oak Ridge National Laboratory, P.O. Box 2008, Oak Ridge, TN 37831-6030, USA*

Received 20 October 1998; accepted 13 January 1999

Abstract

The short superconducting coherence length in high- T_c materials makes them extremely susceptible to the deleterious effect of atomic scale defects. Perhaps the most important of these defects for large-scale technological applications, are grain boundaries. Here we describe an atomic resolution investigation of structural and chemical changes that occur at grain boundaries in high- T_c materials using scanning transmission electron microscopy (STEM). STEM is ideally suited to this analysis, as atomic resolution Z -contrast images and electron energy loss spectra (EELS) can be acquired simultaneously. This permits a direct correlation between the structural images and the local electronic structure information in the spectrum. From this detailed experimental characterization of the grain boundaries, simple theoretical models can be derived that allow the structure-property relationships in high- T_c superconductors to be inferred. Results obtained from $\text{YBa}_2\text{Cu}_3\text{O}_{7-\delta}$ and $(\text{Bi/Pb})_2\text{Sr}_2\text{Ca}_2\text{Cu}_3\text{O}_{10}$ show that there is a charge depletion zone formed at grain boundaries. This charge depletion zone can act as a tunnel barrier to the flow of superconducting charge carriers and appears to increase in width with increasing misorientation angle. The magnitude of the critical current across grain boundaries in high- T_c materials predicted from these models is in excellent agreement with the widely reported electrical transport results. © 1999 Elsevier Science Ltd. All rights reserved.

Keywords: Grain boundaries; Atomic structure; Charge carrier depletion; Scanning transmission electron microscopy (STEM); Electron energy loss spectra (EELS)

1. Introduction

Grain boundaries have long been known to have a deleterious effect on the transport properties of high- T_c superconductors. For example, in systematic studies of high-angle [001] tilt grain boundaries in $\text{YBa}_2\text{Cu}_3\text{O}_{7-\delta}$ (YBCO) thin-film bicrystals, it has been found that there is an exponential decrease in the critical current as the misorientation angle of the boundary increases (Dimos et al., 1990; Gross and Mayer, 1991; Ivanov et al., 1991). While this overall trend in the data is clear, attempts to ascertain the fundamental origin of the transport properties have been confused by the considerable scatter in the experimental measurements (results can vary by several orders of magnitude for the same misorientation angle). Many explanations for the transport properties have been linked to the chemistry of these ceramic oxide materials. It

may be that as YBCO is highly susceptible to the formation of oxygen vacancies, an oxygen deficient boundary layer is formed, thereby reducing the charge carrier concentration (Browning et al., 1992; Zhu et al., 1993; Babcock et al., 1994). Alternatively, there may be second phases, precipitates or the preferential segregation of impurities to the boundary that cause a barrier to transport. However, as all of these possibilities are a function of the processing conditions in ceramic oxides, it is not clear why they should cause the overall trend of an exponential decrease in critical current with misorientation angle. The large scatter in the experimental transport measurements is an obvious consequence of variable processing conditions and the chemistry of the oxide systems, but if it is the dominant effect, high conductivity should be readily achieved by preparing clean, oxygen-rich grain boundaries. This has not been reported in the literature, despite many attempts to oxidize boundaries with excellent cation stoichiometry.

The widely observed transport behavior of grain boundaries in high- T_c superconductors therefore suggests that there is an underlying mechanism responsible for the exponential decrease in critical current with increasing

* Corresponding author. Tel.: + 1-312-413-8164; fax: + 1-312-996-9016.

E-mail address: browning@uic.edu (N.D. Browning)

¹ Current address: University of Birmingham, Birmingham, UK.

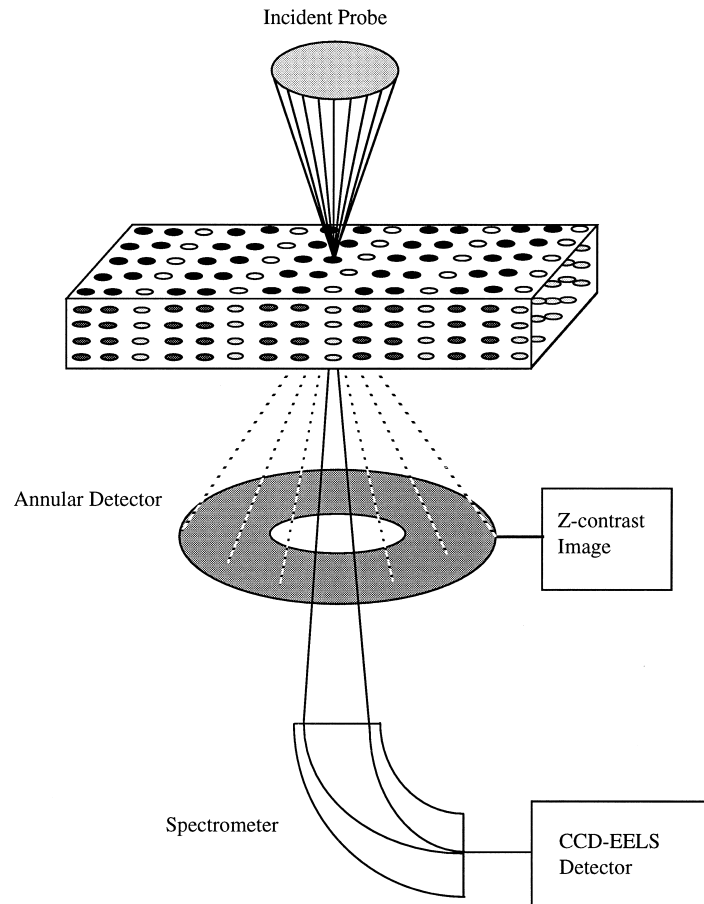


Fig. 1. Schematic of the detector arrangement in the scanning transmission electron microscope (STEM).

misorientation angle. As the superconducting coherence length in these materials is ~ 1 nm, this mechanism is likely to be related to the atomic scale fluctuations in structure and chemistry that can occur at all grain boundaries (even those without second phases). One of the ways to measure these changes on this fundamental atomic scale is through the combination of Z-contrast imaging and electron energy loss spectroscopy (EELS) in the scanning transmission electron microscope (STEM) (Browning et al., 1993a; Batson, 1993). Unlike conventional phase contrast imaging in a transmission electron microscope (TEM), the Z-contrast technique provides a direct image of the structure of grain boundaries that can be intuitively interpreted. Atomic column positions can be determined to be within 0.02 nm accuracy and column compositions inferred from their intensity in the image. Additionally, as the experimental conditions are the same for high-resolution microanalysis, EELS can be acquired from atomic locations defined in the image (see experimental techniques). This spectroscopic technique can detect changes in chemical composition and local electronic structure which can be quantified from variations in the spectral fine-structure (Egerton, 1996; Brydson et al., 1992; Pearson et al., 1988). In particular, core-loss spectra probe transitions from deep core-levels to unoccupied states above the Fermi-level. As each

chemical species and type of bond results in a characteristic position for the Fermi-level and density of unoccupied states, EELS is a very accurate probe of the type of bonding and chemical species present in the material. Therefore, by correlating directly with the atomic structure observed in the Z-contrast image, the structure, composition and chemistry can all be quantified on the atomic scale.

In this article we present results from grain boundaries in $(\text{Bi/Pb})_2\text{Sr}_2\text{Ca}_2\text{Cu}_3\text{O}_{10}$ (Bi-2223) superconducting wires and YBCO thin-film bicrystals. For both materials there is observed to be a charge carrier depletion layer occurring at the grain boundaries. In the case of the less well controlled bulk Bi-2223 system, the presence of extrinsic effects associated with the processing conditions, i.e. second phases and precipitates, is observed. However, in the YBCO thin-films, a charge carrier depletion layer is observed despite the boundaries being stoichiometric. Using crystal chemistry principles, the reason for the charge carrier depletion is determined to be the presence of a reconstructed boundary plane. The boundary reconstruction leads to copper (Cu) sites in the grain boundary plane that are under-coordinated to oxygen (O). As the Cu–O interaction is the essential ingredient to the formation of charge carrying holes in high- T_c materials, this automatically leads to the presence of a carrier depletion zone at the boundary. The

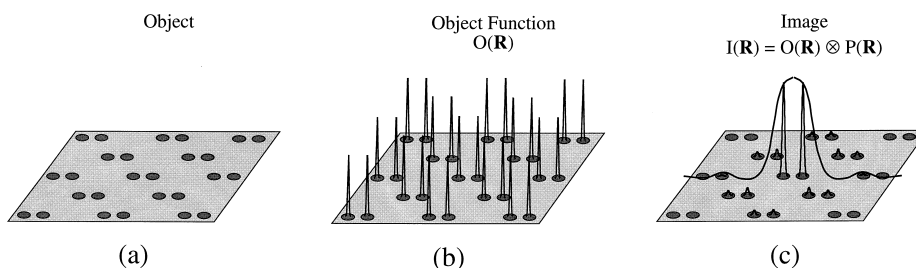


Fig. 2. (a) The specimen consists of an array of atomic columns (b) for which the potential for high-angle scattering can be represented by an object function. (c) The experimental image can be interpreted as a simple convolution of the experimental probe and the object function.

number of under-coordinated sites in the grain boundary plane increases linearly with misorientation angle, naturally explaining the orientation dependence of the transport properties through a tunneling current argument. These models indicate that there is an intrinsic limitation to grain boundary conductivity in high- T_c materials irrespective of processing conditions.

2. Experimental techniques

The results presented in this article were obtained on a VG HB501 dedicated STEM operating at 100 kV with a 0.22 nm probe size, and a VG HB603 dedicated STEM operating at 300 kV with a 0.13 nm probe size. In both of these instruments the electron optics are primarily designed to form a small probe on the surface of the specimen (Fig. 1). The transmitted electrons are collected in a variety of detectors and correlated with the position of the probe as it scans over the surface of the specimen. Obviously, for the electrons to be transmitted through the specimen it must be electron transparent. Specimen thicknesses in the range 10–100 nm were obtained by standard mechanical polishing followed by ion-milling techniques.

2.1. Z-contrast imaging

Z-contrast images (Pennycook and Boatner, 1988; Pennycook and Jesson, 1990; Pennycook and Jesson, 1991; Loane et al., 1992) are formed by collecting the high-angle scattering (75–150 mrad at 100 kV) on an annular detector (Fig. 1). Detecting the scattered intensity at these high-angles and integrating over a large angular range effectively averages coherence effects between neighboring atomic columns in the specimen. Thermal vibrations reduce the coherence between atoms in the same column to residual correlations between near neighbors (Jesson and Pennycook, 1993), a second order effect. This allows each atom to be considered as an independent scatterer. Scattering factors may be replaced by cross sections, and these approach a Z^2 dependence on atomic number. This cross section effectively forms an object function that is strongly peaked at the atom sites, so for very thin specimens where there is no dynamical diffraction, the detected intensity consists of a convolution of this object function with the

probe intensity profile (Fig. 2). The small width of the object function (~ 0.02 nm) means that the spatial resolution is limited only by the probe size of the microscope. For a crystalline material in a zone-axis orientation, where the atomic spacing is greater than the probe size, the atomic columns are illuminated sequentially as the probe is scanned over the specimen. An atomic resolution compositional map is thus generated, in which the intensity depends on the average atomic number of the atoms in the columns.

This result also holds true for thicker specimens. It has previously been noted that for specimens in zone-axis orientations, the STEM probe forms narrow spikes around the atomic columns as it propagates (Fertig and Rose, 1981; Loane et al., 1988). This effect is caused by the coherent nature and large angular spread of the STEM probe, which leads to the tightly bound s-type Bloch states adding constructively and the less localized states interfering destructively (Jesson and Pennycook, 1995). This effect is enhanced for scattering processes such as high-angle thermal diffuse scattering that are localized at the atomic cores, causing a great reduction in beam broadening. With only one dominant Bloch state, dynamical diffraction effects are largely removed and manifest only as a columnar channeling effect, thus maintaining the thin specimen description of the image as a simple convolution of the probe intensity profile and an object function, strongly peaked at the atom sites (Fig. 2).

The phase problem associated with the interpretation of conventional high-resolution TEM images is therefore eliminated. In thin specimens, the dominant contribution to the intensity of a column is always its composition, although due to the higher absorption of the heavy strings the contrast does decrease with increasing specimen thickness and in very thick crystals there is no longer a high resolution image. The effect of changing focus is also intuitively understandable as the focus control alters the probe intensity profile on the surface of the specimen. For defocus less than the optimum Scherzer condition, the probe broadens causing the individual columns not to be resolved. For higher defocus values the probe narrows with the formation of more intense tails, causing sharper image features but compositional averaging over several columns. The optimum focus condition therefore represents a compromise between high resolution (narrow probe profile) and the

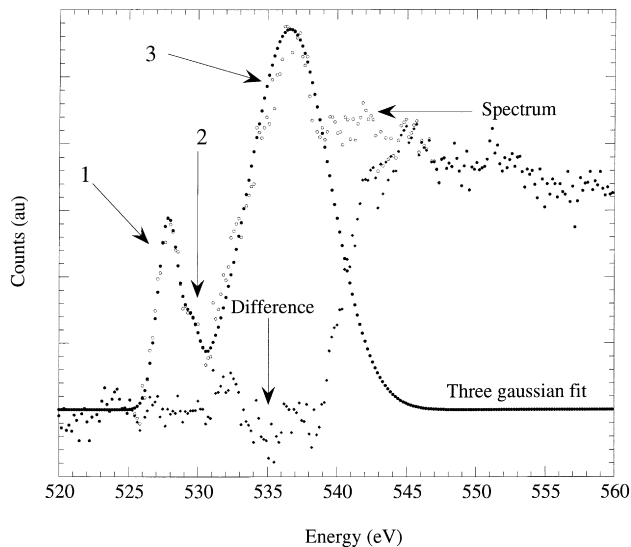


Fig. 3. An example of the three gaussian spectrum fit for a nominally fully oxygenated $\text{YBa}_2\text{Cu}_3\text{O}_{7-\delta}$ sample, i.e. $\delta = 0$. The intensity of first pre-edge feature is an accurate representation of the number of holes in the valence band (Browning et al., 1992). To make the quantification independent of experimental conditions and specimen thickness, the intensity in the peak is normalized with the gaussian fitted to the main edge.

desire for a highly local image (no significant tails to the probe). This also corresponds to the optimum probe for microanalysis.

At defects and interfaces, structures can become extremely complicated, causing difficulties in determining the precise 3-dimensional composition. However, provided an atomic column is continuous through the crystal, reconstructions will only result in a change in column intensity and not a contrast reversal. The atomic structure in the region of defects and interfaces can therefore still be determined largely from the image, and used to position the electron probe for EELS (Browning et al., 1993a; Batson, 1993).

2.2. Electron energy loss spectroscopy

As can be seen from Fig. 1, the annular detector used for Z-contrast imaging does not interfere with the low-angle scattering used for electron energy loss spectroscopy. This means that the Z-contrast image can be used to position the electron probe over a particular structural feature for acquisition of a spectrum. To be able to correlate the spectrum precisely with the structural feature, it is essential that the spectrum have the same atomic resolution as the Z-contrast image. In order to achieve this atomic resolution, the range over which a fast electron can cause an excitation event must be less than the interatomic spacing. Hydrogenic models (Allen and Rossouw, 1990) show that for the majority of edges accessible by conventional energy-loss spectrometers ($\Delta E < 2 \text{ keV}$) the object functions are localized within 0.1 nm of the atom cores (Pennycook et al., 1995; Browning and Pennycook, 1995; Holbrook and Bird, 1995).

Hence, like the Z-contrast image, we have an object function localized at the atom cores and an experimental probe of atomic dimensions. For crystalline materials in zone-axis orientations, providing we maintain a large collection angle (15–30 mrad), coherent effects will be averaged and the description of the spectrum in terms of a convolution of the probe with an object function is valid (Fig. 2). An important aspect of this experimental approach is that the probe channeling discussed for Z-contrast imaging will also preserve the spatial resolution of the spectrum, thereby allowing atomic resolution analysis of the electronic structure to be achieved even with large collection apertures. Of course specimen drift is also a problem, but for the acquisition times of less than 5 s used here, the 1 Å/min drift of the microscope does not induce a significant broadening effect.

The electronic structure of high- T_c superconductors has been extensively studied over the last ten years. In the case of p-type superconducting compounds, such as YBCO and Bi-2223, the doping mechanism can be explained by considering the structure to consist of conduction CuO_2 layers separated by charge reservoir blocks. The interaction of the charge reservoir blocks with the conduction layers leads to the formation of the charge carrying holes in the predominantly Oxygen 2p–Copper 3d valence band. As electron energy loss spectroscopy is sensitive to the density of unoccupied states in the region of the Fermi surface, this means a quantified measurement of the number of charge carriers can in principle be obtained from both oxygen and copper core-edge spectra. For EELS in the electron microscope, the characteristic core edges that are readily accessible by the spectrometer are the oxygen K-edge (1s \rightarrow 2p transitions) and the copper $L_{2,3}$ -edge (2p \rightarrow 3d transitions). For YBCO, the most accurate means of quantifying the number of holes is through the pre-edge feature on the oxygen K-edge (Browning et al., 1992) using a series of Gaussian functions (Fig. 3). This quantification allows the hole concentration to be determined to $\sim 5\%$ accuracy. For Bi-2223, the features on the oxygen K-edge are less well defined (due to a lack of high-quality standard spectra) and analysis in this paper is limited to the copper $L_{2,3}$ edge (Prouteau et al., 1998). However, in both cases the Z-contrast image can be used to position the electron probe over a particular grain boundary to probe the local charge carrier density and, ultimately, correlate the structure with the electronic properties of the boundary.

3. Results

3.1. $(\text{Bi/Pb})_2\text{Sr}_2\text{Ca}_2\text{Cu}_3\text{O}_{10}$

The Bi-2223 materials examined in the STEM (Prouteau et al., 1998) were 19 filament composites fabricated at American Superconductor Corporation (ASC) using the powder-in-tube technique (Li et al., 1997) with a powder stoichiometry of $\text{Bi}_{1.7}\text{Pb}_{0.3}\text{Sr}_{1.9}\text{Ca}_2\text{Cu}_{3.1}\text{O}_x$. A thermomechanical process

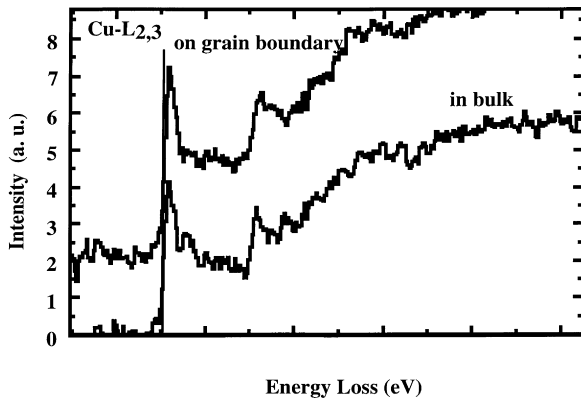


Fig. 4. Comparison of the copper- $L_{2,3}$ edge from low angle grain boundaries with the bulk spectrum from a nearby region in a Bi-2223 tape ($J_c = 30 \text{ kA/cm}^2$ at 77 K). No difference is observed between the bulk and the grain boundary.

consisting of a sequence of roll deformation and heat treatment steps was used to promote Bi-2223 phase formation, texture, and densification. Transport critical current ($1 \mu\text{V/cm}$) measurements at 77 K under self-field were performed at ASC using a standard four probe technique. Two tapes with different properties have been investigated in order to correlate critical current density and microstructure. They have respectively critical current densities (J_c) of 30 kA/cm^2 and 46 kA/cm^2 .

For both the tapes, low-angle grain boundaries ($\sim 5^\circ$) are ubiquitous within all the filaments. Spectra were recorded from a number of boundaries located near the silver-filament interface. Unfortunately due to the limited $\pm 6^\circ$ tilt capability of the microscope, it was impossible to tilt the specimen exactly to the zone axis. Therefore we were not able to record spectra from individual cores and cannot draw definitive conclusion concerning the quality of the cores. However, no difference was found between the copper- $L_{2,3}$ spectra recorded from the bulk and those recorded from several low angle grain boundaries, where the contributions of both cores and inter-core regions are included (Fig. 4). This reflects the absence of extended region along the low angle grain boundaries where the electronic structure is significantly different from the bulk.

In the lower J_c tape, a great number of Ca, Pb-rich precipitates are associated with the presence of high-angle grain boundaries. The diameter of these precipitates varies from 2 to 20 nm, as shown in the low resolution Z-contrast image (Fig. 5(a)). From the image intensity and from EELS, these precipitates are found to be rich in calcium and lead. The copper- $L_{2,3}$ edge and at the oxygen-K edge have been recorded in the bulk and around several precipitates located at high angle grain boundaries. Spectra representative of the boundaries decorated with these precipitates are shown in Fig. 5(b). Again, comparing the spectra to the bulk, the copper $L_{2,3}$ edge shows significant changes, indicating that the electronic structure of the boundary is not the same as the bulk. It is also important to note that none of the

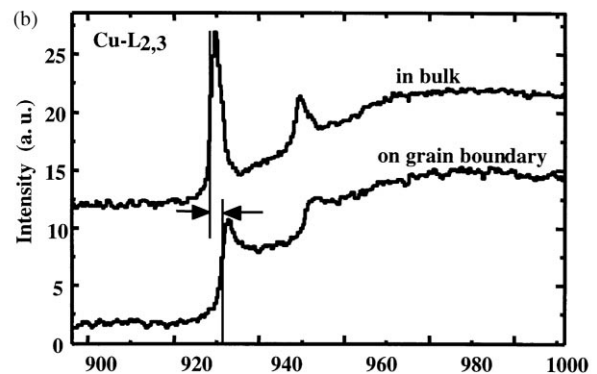
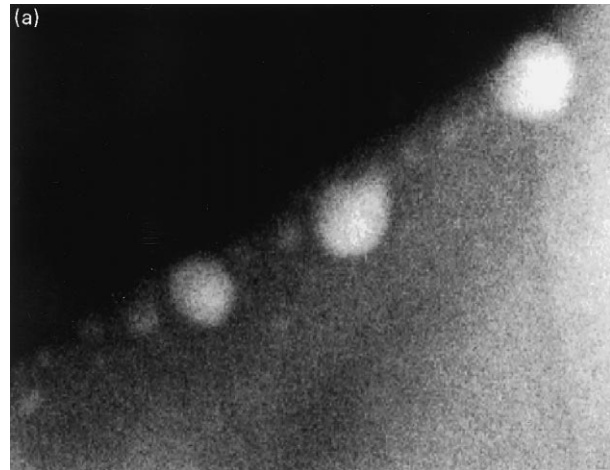


Fig. 5. Z-contrast image (a) of precipitates at a high angle grain boundary and in the bulk region nearby in Bi-2223. The precipitate's brightness and the EELS analysis suggest that they are calcium and lead rich. (b) shows the copper- $L_{2,3}$ edge in the region of the precipitates and in the bulk of a Bi-2223 tape ($J_c = 30 \text{ kA/cm}^2$ at 77 K).

precipitates were found at the low-angle grain boundaries. In the higher J_c tape, the high-angle grain boundaries are found to be free from precipitates with copper- $L_{2,3}$ spectra that are similar to the low-angle grain boundaries (Fig. 6).

3.2. $YBa_2Cu_3O_{7-\delta}$

Fig. 7 shows a Z-contrast image of a low-angle YBCO grain boundary and Fig. 8 shows a YBCO 30° [001] asymmetric tilt boundary grown by laser ablation on a SrTiO_3 bicrystal substrate. In the images, the brighter columns consist of Y and Ba atoms, and the less bright columns consist of Cu(1), Cu(2) and O(4) atoms. Columns consisting of solely oxygen atoms, i.e. those containing O(2) or O(1) and O(3) atoms, scatter too little to contribute to the image. These high-resolution images show that both the low- and high-angle boundaries contain the same structural units (Browning et al., 1998a). Additionally, neither of the boundaries showed the presence of second phases or segregated impurities. These images were acquired with the HB603 dedicated STEM that is not equipped with EELS capabilities. However, using the HB501 to perform spatially

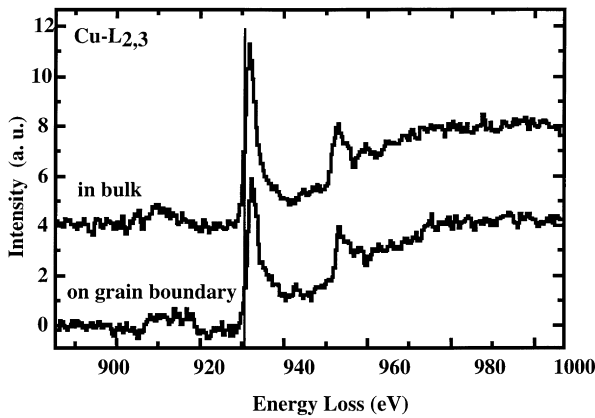


Fig. 6. The copper- $L_{2,3}$ edge at a high angle grain boundary and in the bulk nearby in a Bi-2223 tape ($J_c = 45 \text{ kA/cm}^2$ at 77 K). In this case no precipitates were observed and no difference is observed between the bulk and the grain boundary, indicating no depletion zone.

resolved energy loss spectroscopy on a 30° asymmetric boundary in a polycrystalline YBCO sample produced by laser ablation (Browning et al., 1993b), resulted in the carrier concentration profile shown in Fig. 9. Here, oxygen K-edge spectra were recorded in 0.4 nm steps across the grain boundary and the pre-edge intensity quantified using the 3 gaussian method (Fig. 3). As can be clearly seen from the profile, the carrier concentration is greatly depleted even at this clean boundary.

4. Discussion

The results from the two systems show that in both cases there can be significant changes in the local electronic structure at high-angle grain boundaries. However, if we consider the processing mechanism involved with each sample, it is reasonably straightforward to see that the origin of the electronic structure changes is different in the two cases. In the case of the Bi-2223 wires, the bulk processing methods mean that the grain boundaries are much more likely to be decorated with precipitates and second phases. This means that the gross changes in the local electronic structure are related to an extrinsic effect at the grain boundaries, i.e. the boundaries are not stoichiometric. However, in the case of YBCO, the laser ablation method of producing the thin films results in a clean grain boundary plane with excellent cation stoichiometry. The changes in the fine structure in this case are therefore related to either an intrinsic effect at the grain boundary or possibly oxygen deficiency (see later). In attempting to draw some general conclusions as to the effect that the observed electronic structure changes will have on the transport properties of the grain boundaries it is therefore convenient to split the discussion into extrinsic and intrinsic properties. In this regard, we shall first consider the results from the Bi-2223

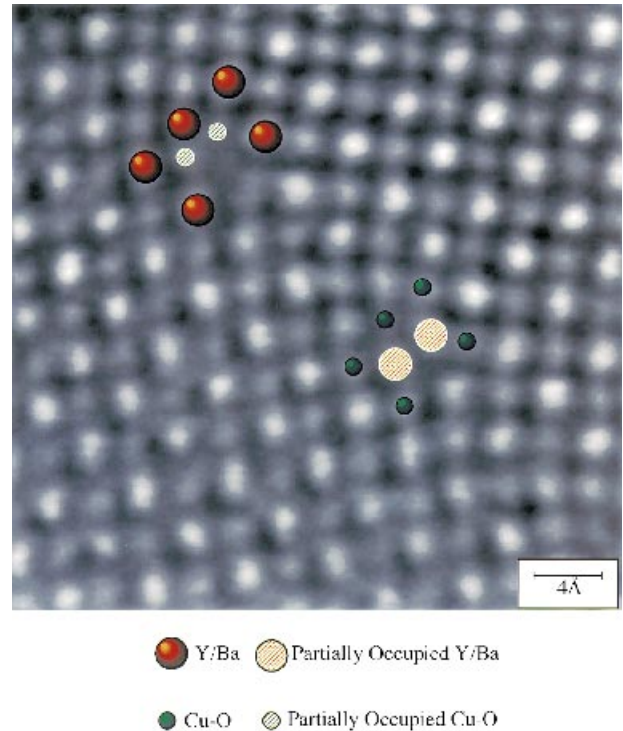


Fig. 7. Z-contrast image of a low-angle [001] tilt boundary in YBCO obtained from a 300 kV VG Microscopes HB603 dedicated STEM. The Z-contrast in the image allows the sub-lattice, i.e. Cu or Y/Ba on which the dislocation core reconstruction forms to be identified.

grain boundaries, i.e. the extrinsic properties of grain boundaries.

To interpret the electronic structure changes in terms of the properties of the boundaries in Bi-2223, we must first examine the origin of changes in the fine structure of the Cu $L_{2,3}$ edge. The $L_{2,3}$ -edges in transition metal elements, such as copper, are characterized by the presence of two sharp features or “white lines”. The separation of these white lines is determined by the spin-orbit splitting of the initial state, while their intensity ratio in a simplistic model is related to the number of electrons in the final states of the transition, i.e. 3d states (Egerton, 1996). For metallic copper, the 3d band is filled and the spectrum shows no white lines. As the oxidation state of copper is increased the intensity of the white lines increases. Hence we can use the intensity of the white lines in the copper $L_{2,3}$ -edge as an estimation of the copper oxidation state. In the p-type superconductors, the formal copper oxidation state in the superconducting phase is between +2 and +3 and the Cu $L_{2,3}$ -edge should have the signature intense white lines. Accurate quantification of the copper valence from the white lines is, however, not a straightforward proposition. The simplistic argument of intensity being proportional to 3d occupancy is known to have exceptions (Egerton, 1996). Additionally, the methodology used to subtract the background and measure the intensity of the white lines is subject to experimental errors. As such, using this technique as it stands now, we would not expect to be able to quantify the Cu 3d occupancy to within

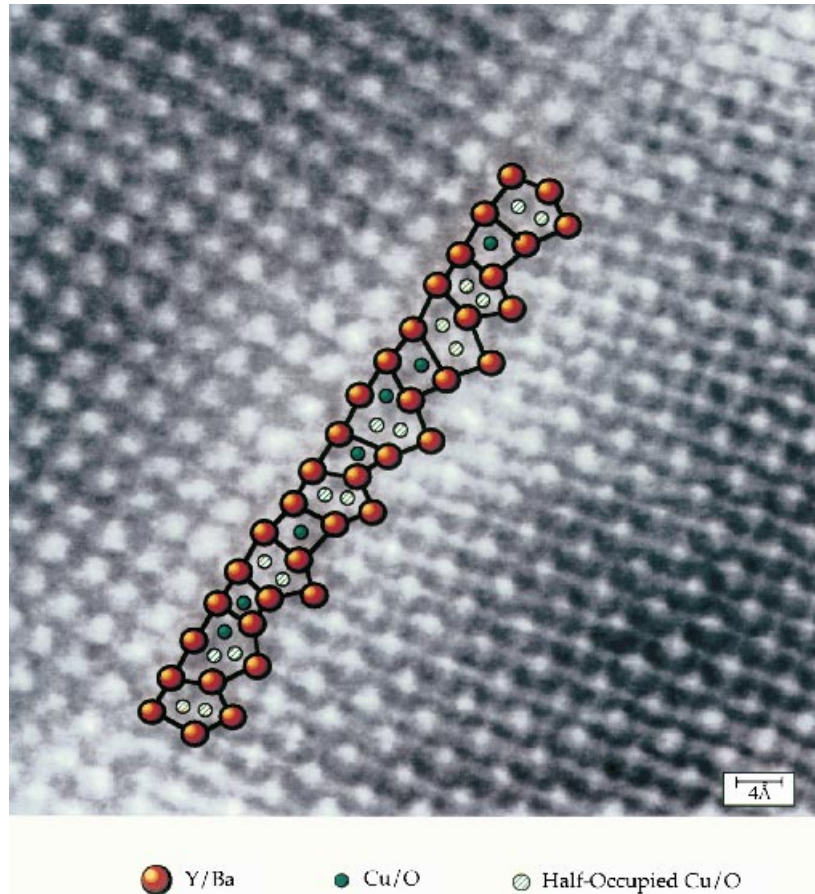


Fig. 8. Z-contrast image of a 30° [001] YBCO tilt boundary obtained from a 300 kV VG Microscopes HB603 dedicated STEM.

15%. Therefore, in the following discussion we will use the white line intensity as a fingerprint in relation to the intensity seen in the bulk spectra.

The white line intensities in the copper-L_{2,3} absorption edges recorded in the bulk of both tapes is consistent with the average copper valence being in the range from + 2 to + 3, i.e. the bulk grains are superconducting. The spectra recorded from low-angle grain boundaries close to the Ag-interface also have the intense white line signature and there is virtually no difference between their spectra and those of the bulk. This is consistent with the results obtained using magnetic imaging techniques, where it was found that the majority of the superconducting current flows through grains close to the Ag-interface (Pashitskii et al., 1995). In the lower J_c wire, there is a great reduction in the intensity of the white lines at the high-angle grain boundaries near the center of the filaments. Interpreting this as a filling of the empty copper 3d states, suggests that the boundaries contain copper in a much reduced oxidation state. In fact, the white line intensities are consistent with the average copper oxidation state being + 1 or less. It is therefore clear from the copper spectra that these boundaries are non-superconducting. At the high-angle boundaries in the higher J_c wire, the copper L_{2,3}-edge exhibits white line intensities comparable to the bulk spectra. These boundaries therefore contain more

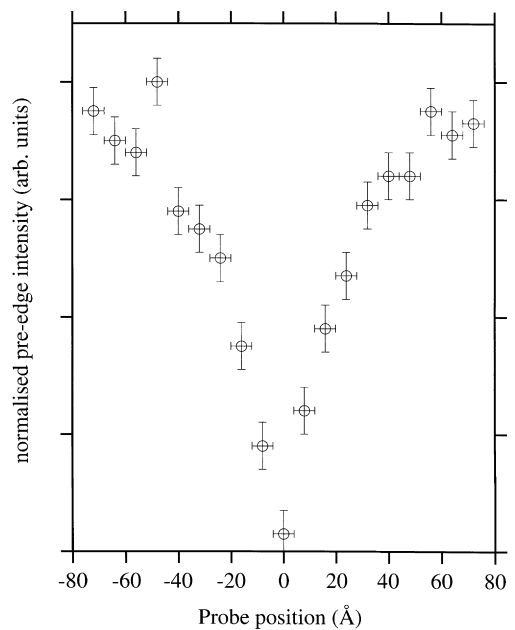


Fig. 9. Quantifying the change in pre-edge intensity by a normalised gaussian fit, shows that within the errors of the experiment there is a hole depletion zone extending 50–60 Å either side of the 30° asymmetric boundary.

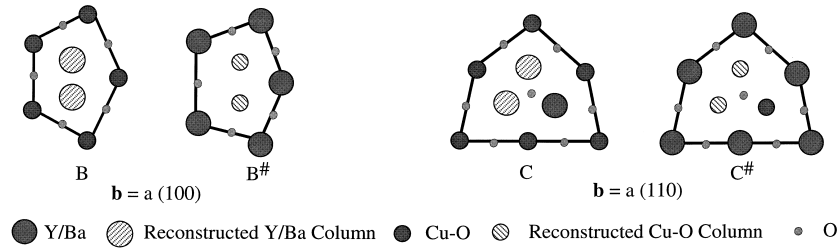


Fig. 10. Structural units for [001] tilt boundaries in YBCO.

unoccupied copper 3d states and we can expect such boundaries to show better transport behavior.

These results indicate that a “non-superconducting” area close to grain boundaries can easily be related to non-stoichiometry, i.e. the Ca, Pb-rich precipitates. If there is an extended non-stoichiometric region with a width larger than the superconducting coherence length, this must contribute to a low critical current density across grain boundaries. However, what is also clear from the results is that processing can affect the non-stoichiometry at the grain boundaries. In the higher J_c wire, high-angle grain boundaries show much fewer precipitates than the lower J_c wire and correspondingly more “bulk-like” copper valence. However, at this stage the sensitivity of the 3d occupancy measurement is not sufficient to determine whether such boundaries are “good” for transport. Even a small change ($< 1\%$) in the copper 3d occupancy can lead to the presence of weak links. While work is continuing in an attempt to address an accurate determination of local electronic structure of stoichiometric grain boundaries in Bi-2223, to examine the intrinsic effects of the grain boundaries in high- T_c materials here, we must now consider the results from YBCO. (It must be noted that non-stoichiometry at YBCO boundaries will also have the effect of reducing the copper valence and creating a non-superconducting boundary plane.)

The YBCO thin film grain boundaries produced by laser ablation are known to be free from second phases, impurities and copper enrichment (Browning et al., 1993b). The reduction in the critical current at grain boundaries in these materials must therefore either be an intrinsic consequence of the grain boundary misorientation angle or caused by oxygen deficiency. Unfortunately, discriminating between oxygen deficiency and charge carrier depletion due to the grain boundary plane is not straightforward. The 3 gaussian fitting routine described in the experimental section measures the hole concentration directly. However, the formation of the charge carrying holes in bulk YBCO is controlled by the oxygen occupancy in the Cu–O chains. Therefore, any oxygen depletion at the grain boundary will immediately decrease the number of charge carriers (holes) and have an effect on the oxygen spectrum. Although it is in principle possible to independently measure the oxygen concentration through the integrated intensity in the oxygen K-edge, the accuracy is limited to $\sim 15\%$ (see discussion on

the quantification of the copper $L_{2,3}$ edge). As a change in oxygen concentration of only 8% is sufficient for YBCO to go from superconducting to insulating, the required sensitivity is not available with this method. In order to analyze the intrinsic effect of the grain boundary plane, we will therefore assume in the following discussion that the YBCO grain boundary is fully oxygenated. This is a reasonable assumption in attempting to ascertain the intrinsic properties of the grain boundaries in light of the experimental evidence showing that no amount of oxidation can increase the J_c of grain boundaries up to the bulk levels (Moeckly et al., 1993).

The images obtained from the grain boundaries in YBCO (Figs. 7 and 8) show that the low and high-angle grain boundaries are composed of similar “structural units”. The structural unit model (Sutton and Vitek, 1983; Browning and Pennycook, 1996) is an alternate methodology of describing grain boundary structures that is formally equivalent to the dislocation core model. However, the structural unit model for high-angle grain boundaries has the advantage that once the structural units have been determined, it is possible to predict the structure of a grain boundary at any misorientation. For YBCO, the structural units needed to construct any [001] tilt boundary are shown in Fig. 10 (Browning et al., 1998a). As can be seen from

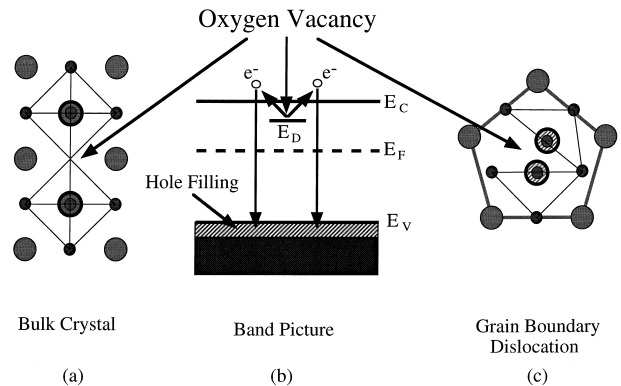


Fig. 11. (a) Reduced atomic coordination of copper atoms in the bulk due to an oxygen vacancy, (b) results in donor states being formed near the conduction band edge and (c) recombination of these electrons with holes in the valence band reduces the number of free charge carriers. A similar reduced coordination is present in the dislocation cores of the grain boundary. These *effective* vacancies can not be filled as there is insufficient space for an oxygen atom.

Table 1

The distinct grain boundary structural units of Fig. 10 can be combined to construct all [001] tilt boundaries in YBCO by applying the “strip method” (Sutton, 1988). As asymmetric grain boundaries are only quasi-periodic, we must define two units that are composed of the different structural units shown in Fig. 10. The graphical “strip method” then allows us to combine these units in a manner consistent with the misorientation angle to form the boundary plane. Assuming that each of the structural units results in one under-coordinated copper site, the density of localized boundary states can be calculated

Boundary plane	Unit 1	Unit 2	Boundary structure	Localized states.m ³
(100) ₁ /(510) ₂	(AAAAB) ₉ (AAAAC)	(AAAAB) ₁₀ (AAAAC)	(1) ₁₀ (2)(1) ₉ (2)(1) ₉ ...	8.6 × 10 ¹⁷
(100) ₁ /(410) ₂	(AAAB) ₈ (AAAC)	(AAAB) ₉ (AAAC)	(1) ₈ (2)(1) ₇ (2)(1) ₇ ...	1.1 × 10 ¹⁸
(100) ₁ /(310) ₂	(AAB) ₆ (AAC)	(AAB) ₇ (AAC)	(1) ₆ (2)(1) ₅ (2)(1) ₅ ...	1.4 × 10 ¹⁸
(100) ₁ /(210) ₂	ABABABAC	ABABABABAC	(1) ₄ (2)(1) ₃ (2)(1) ₃ ...	2.0 × 10 ¹⁸
(100) ₁ /(320) ₂	ABC	ABBABC	1212212122121...	2.5 × 10 ¹⁸
(100) ₁ /(110) ₂	BC	BBC	BBCBCBBCBC...	3.5 × 10 ¹⁸

Fig. 10, the structural unit model allows for the fact that the dislocation cores can form on either of the cation sub-lattices. This is not included in dislocation core models where the Burger’s vector is used as the only classification. Whether the dislocations are formed on the copper sub-lattice or the Y/Ba sub-lattice is obviously important for YBCO, where the formation of charge carrying holes is dependent on the oxygen 2p-copper 3d hybridization. As can be seen from Fig. 7, in low-angle grain boundaries both types of dislocation cores are observed. However, for high-angle asymmetric grain boundaries, like the one shown in Fig. 8, the structural units seem universally to be centered on the copper sub-lattice. As high-angle grain boundaries in YBCO have been found to contain predominantly asymmetric facet structures (Kabius et al., 1994; Browning et

al., 1998a), we shall consider only these structural units in the following discussion.

One interesting feature of both cores is that there exist atomic locations where the columns appear too close together. In such situations, like-ion repulsion would be expected to preclude such a structure. However, if we remember that the Z-contrast image, like any transmission image, is simply a 2-dimensional projection of the 3-dimensional crystal structure, a solution to this problem is for only one of the two sites in each perovskite block to be occupied. If alternate sites are chosen, we would still see two columns in projection but avoid like-ion repulsion. An alternative view of these two “half-columns” is that they represent a single atomic column that is distorted through the thickness of the crystal in a regular manner, i.e. a 2 × 1 dislocation core reconstruction. This reconstruction has been shown to be a valid structure in the perovskite SrTiO₃ (Browning and Pennycook, 1996; Wallis and Browning, 1997; Ravikumar, 1996; Browning et al., 1998b) and it is reasonable to assume that the same applies here.

Having defined the structural units in this way it is relatively straightforward to make a simple interpretation of the properties of each of these units. Fig. 11 shows that each of the reconstructed columns results in the copper atoms in the boundary core being under-coordinated to oxygen. If this occurred in the bulk of the material, we would say that there is an oxygen vacancy (deficiency) which results in localized donor states (each missing oxygen 2 – ion means there are two electrons in the system). Changing the equilibrium charge concentration in this manner should lead to recombination, which would then result in a reduction in the charge carrier (hole) concentration, i.e. the superconducting properties would be reduced. As a first approximation, we can say the same thing here for the boundary. However, unlike the bulk material, in this case the oxygen vacancy is not a real vacancy. In the bulk material, we could potentially fill the oxygen vacancy through further oxygenation of the sample, i.e. it is dependent on processing. At the grain boundary there is not enough space between the copper columns to accommodate an additional oxygen atom (Browning et al., 1998b). The grain boundary plane therefore contains an intrinsic arrangement of under-coordinated atoms and no amount of processing can overcome the hole

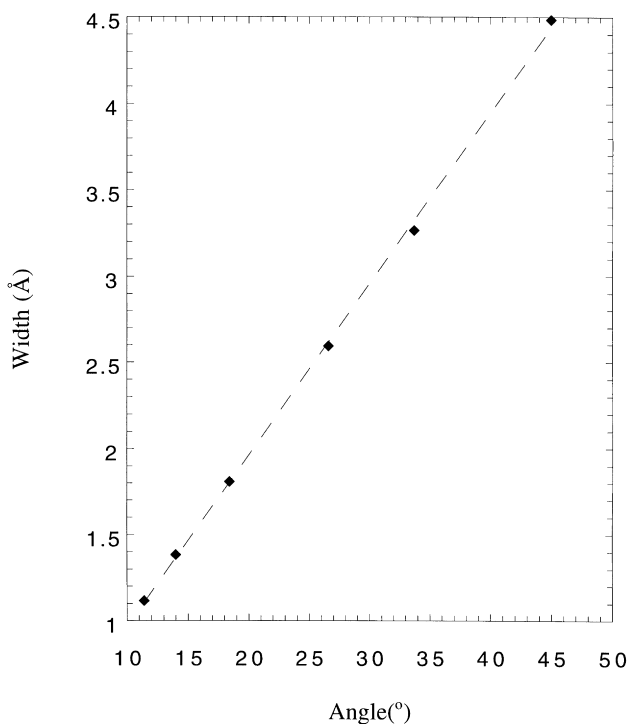


Fig. 12. The width of the depletion layer as a function of the misorientation angle calculated from Eq. 1 and using the number of localized boundary states in Table 1. There is a linear increase in the width of the carrier depletion zone with misorientation angle.

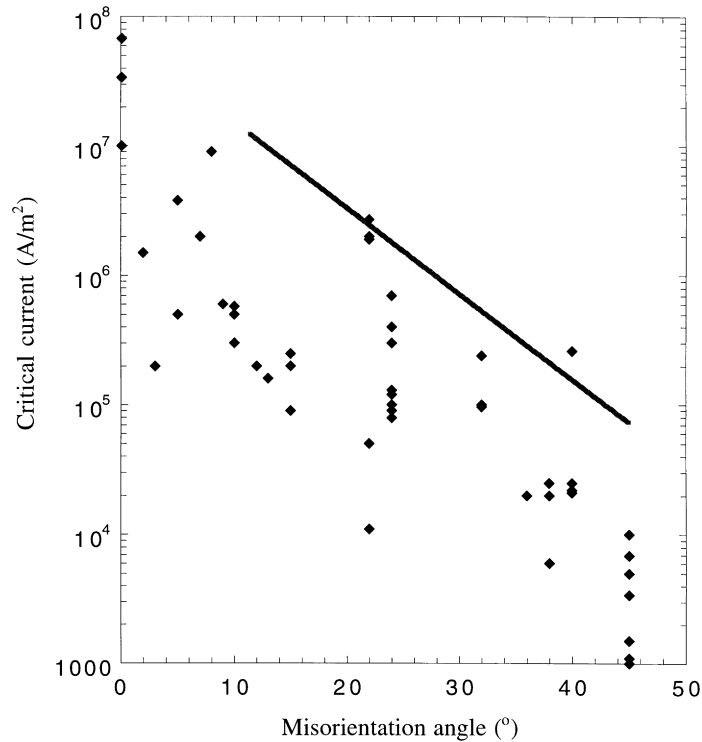


Fig. 13. Experimental observations of J_c ($T = 4.2$ K) as a function of misorientation angle taken from the results of several groups (Dimos et al., 1990; Gross and Mayer, 1991; Ivanov et al., 1991) show an exponential dependence. In cases where the results were reported at $T = 77$ K, the values at 4.2 K were extrapolated from the temperature dependence of J_c (Mannhart et al., 1988). The grain boundary tunneling current, calculated from Eq. (2) using the grain boundary widths from Fig. 12, shows excellent quantitative agreement with the underlying exponential dependence.

depletion caused by this reconstructed grain boundary plane. Second phases and precipitation will only make transport worse, not better. This is consistent with the observed transport properties.

As we stated earlier, one of the advantages of the structural unit model is that it allows us to predict the grain boundary structure at any misorientation angle. This also applies to the asymmetric grain boundary structures under discussion here, even though they are only quasi-periodic. Using the “strip-method” (Sutton, 1988; Browning and Pennycook, 1996), the grain boundary repeat structures for various misorientation angles are shown in Table 1. If we assume that each of the structural units contains one under-coordinated site, then it is possible to calculate the number of donor states at the boundary plane as a function of misorientation angle. As can be clearly seen from Table 1, the number of localized donor states in the grain boundary increases with the misorientation angle.

In the normal state, i.e. above the transition temperature, fully oxygenated YBCO is a semiconductor. The electrical properties of semiconductor grain boundaries in the presence of localized donor/acceptor states is well defined (Sutton and Balluffi, 1995). The localized states in the boundary plane are considered to be a 2-dimensional plane of charge, which is compensated by a charge depletion zone either side of the grain boundary plane. The width of this depletion zone can be calculated from the equation

(Sutton and Balluffi, 1995):

$$S_{\text{gb}} = N_{\text{bulk}} w \quad (1)$$

where S_{gb} is the number of localized boundary states, N_{bulk} is the bulk carrier doping and w is full width of the depletion zone. Inserting the values for the localized boundary charge shown in Table 1 and using the bulk doping value of $\sim 10^{21}/\text{cm}^3$ (Mannhart and Hilgenkamp, 1998), we can calculate the depletion width. As can be seen from Fig. 12, the width of the depletion zone increases linearly with misorientation angle.

Asymmetric high-angle grain boundaries therefore have an intrinsic boundary width where the material is devoid of free charge carriers. As was stated earlier, for thin films of YBCO grown on bicrystal substrates, the boundaries facet with predominantly asymmetric boundary planes. It is therefore reasonable to assume that the experimental transport measurements across high-angle grain boundaries were dominated by transport across these asymmetric facets. At these boundaries the current must flow by tunneling across the non-superconducting barrier. The magnitude of the tunneling current across a barrier can be calculated from (Halbritter, 1992):

$$J_c = J_{c0} \exp(-2\kappa\Delta) \quad (2)$$

where J_{c0} is the bulk critical current, Δ is the interface width and κ is the decay constant (7.7/nm) (Halbritter, 1992). For

each of the grain boundary misorientations above, the width can be used to determine the expected tunneling current for a constant applied voltage, the criterion used experimentally to measure critical currents. In Fig. 13, the tunneling current as a function of misorientation angle for asymmetric boundaries is plotted and compared with a range of experimental critical current measurements (Dimos et al., 1990; Gross and Mayer, 1991; Ivanov et al., 1991). For the boundary widths defined above, the structural unit model quantitatively reproduces the trend of exponentially decreasing critical current with increasing misorientation angle. The fact that the line goes through the highest values of the experimental data is to be expected as in this analysis we have only considered the intrinsic effect of the boundary. If we were to add the effect of processing induced oxygen deficiency, the charge depletion width would obviously increase thereby lowering the critical current. The effect of further oxygen deficiency is shown in the EELS profile of Fig. 9. Here the width of the hole depletion zone is much broader than the intrinsic width calculated in Table 1. This should not be surprising considering the degree of specimen preparation needed to prepare an electron transparent sample. Additionally, as can be seen from the Bi-2223 results, second phases also lead to considerable hole depletion. Again, the presence of processing induced second phases would lower the critical current.

5. Conclusions

The results from both Bi-2223 and YBCO show that there can be large changes in the local electronic structure associated with grain boundaries. The most prominent changes occur when there is a stoichiometry change at the grain boundary associated with a second phase, precipitate, segregated impurity or oxygen deficiency. Analysis of the intrinsic structure of the clean, stoichiometric grain boundaries indicates that there exists a reconstructed boundary plane. This boundary reconstruction, that has been shown to be the low-energy structure in similar structured perovskites (Ravikumar, 1996), results in under-coordinated copper atoms in the boundary plane. The under-coordination of these sites can be considered to be the equivalent of immobile oxygen vacancies in the boundary plane, and results in a compensating charge depletion zone. As the density of reconstructed sites increases linearly with misorientation angle, this naturally leads to a linear increase in the width of the depletion zone. Assuming that the limitation on the critical current across grain boundaries is tunneling across the depletion zone accurately reproduces the experimental observations. These results show that grain boundaries in high- T_c superconductors are intrinsically limited in the critical current that can be carried across them.

Acknowledgements

Aspects of this work were performed in collaboration

with M.F. Chisholm, P.D. Nellist, M. Teplitsky and G.N. Riley Jr. This research is funded by NSF under grant No's. DMR-9503877 and DMR-9803021, by the US DOE under contract no. DE-ACOS-96OR22464 with Lockheed Martin Energy Research Corporation and by a partial appointment to the ORNL postdoctoral program administered by ORISE.

References

- Allen, L.J., Rossouw, C.J., 1990. Absorptive potentials due to ionisation and thermal diffuse scattering by fast electrons. *Phys Rev B* 42, 11 644–11 654.
- Babcock, S.E., Cai, S.Y., Larbalestier, D.C., Shin, D.H., Zhang, N., Zhang, H., Kaiser, D.L., Gao, Y., 1994. A TEM-EELS study of hole concentrations near strongly and weakly coupled grain boundaries in electromagnetically characterized $\text{YBa}_2\text{Cu}_3\text{O}_{7-\delta}$ bicrystals. *Physica C* 227, 183–196.
- Batson, P.E., 1993. Simultaneous STEM and electron energy loss spectroscopy with atomic column sensitivity. *Nature* 366, 727–729.
- Browning, N.D., Yuan, J., Brown, L.M., 1992. Determination of local oxygen stoichiometry in $\text{YBa}_2\text{Cu}_3\text{O}_{7-\delta}$ by electron energy loss spectroscopy in the scanning transmission electron microscope. *Physica C* 202, 12–18.
- Browning, N.D., Chisholm, M.F., Pennycook, S.J., 1993. Atomic resolution chemical analysis in the scanning transmission electron microscope. *Nature* 366, 143–146.
- Browning, N.D., Chisholm, M.F., Norton, D.P., Lowndes, D.H., Pennycook, S.J., 1993. Correlation between hole depletion and atomic structure at high-angle $\text{YBa}_2\text{Cu}_3\text{O}_{7-\delta}$ grain boundaries. *Physica C* 212, 185–190.
- Browning, N.D., Pennycook, S.J., 1995. Atomic resolution electron energy loss spectroscopy in the scanning transmission electron microscope. *J. Microsc.* 180, 230–237.
- Browning, N.D., Pennycook, S.J., 1996. Direct experimental determination of the atomic structure at internal interfaces. *J. Phys. D* 29, 1779–1798.
- Browning, N.D., Buban, J.P., Nellist, P.D., Norton, D.P., Pennycook, S.J., 1998. The atomic origins of reduced critical currents at [001] tilt grain boundaries in YBCO thin films. *Physica C* 294, 183–193.
- Browning, N.D., Moltaji, H.O., Buban, J.P., 1998. Investigations of 3-D grain boundary structures in oxides through multiple scattering analysis of spatially resolved electron energy loss spectra. *Phys. Rev. B* 58, 8289–8300.
- Brydson, R., Sauer, H., Engle, W., 1992. Electron energy loss near edge structure as an analytical tool—the study of minerals. In: Disko, M.M., Ahn, C.C., Fultz, B. (Eds.). *Transmission Electron Energy Loss Spectrometry in Materials Science, The Minerals, Metals and Materials Society, Warrendale, PA*, pp. 131–154.
- Dimos, D., Chaudhari, P., Mannhart, J., 1990. Superconducting transport properties of grain boundaries in $\text{YBa}_2\text{Cu}_3\text{O}_{7-\delta}$ bicrystals. *Phys. Rev. B* 41, 4038–4049.
- Egerton, R.F., 1996. *Electron Energy Loss Spectroscopy in the Electron Microscope*, Plenum Press, New York.
- Fertig, J., Rose, H., 1981. Resolution and contrast of crystalline objects in high-resolution scanning transmissions electron microscopy. *Optik* 59, 407–429.
- Gross, R., Mayer, B., 1991. Transport processes and noise in $\text{YBa}_2\text{Cu}_3\text{O}_{7-\delta}$ grain boundary junctions. *Physica C* 180, 235–242.
- Halbritter, J., 1992. Pair weakening and tunnel channels at cuprate interfaces. *Phys. Rev. B* 46, 14861–14871.
- Holbrook, O.F., Bird, D.M., 1995. Theoretical modelling of the size and shape of atomic images formed with inelastically scattered electrons. *Proc. Microscopy and Microanalysis 1995*, 278–279.
- Ivanov, Z.G., Nilsson, P.A., Winkler, D., Claeson, T., Stepanov, E.A., Tzalenchuk, A.Ya., 1991. Weak links and dc SQUIDS on artificial

- nonsymmetric grain boundaries in $\text{YBa}_2\text{Cu}_3\text{O}_{7-\delta}$. *Appl. Phys. Lett.* 59, 3030–3032.
- Jesson, D.E., Pennycook, S.J., 1993. Incoherent imaging of thin specimens using coherently scattered electrons. *Proc. R. Soc. Lond. A* 441, 261–281.
- Jesson, D.E., Pennycook, S.J., 1995. Incoherent imaging of crystals using thermally scattered electrons. *Proc. R. Soc. Lond. A* 449, 273–293.
- Kabius, B., Seo, J.W., Amrein, T., Dahne, U., Scholen, A., Siegel, M., Urban, K., Schultz, C., 1994. Grain boundary structure of thin films of $\text{YBa}_2\text{Cu}_3\text{O}_7$ and $\text{Bi}_2\text{Sr}_2\text{CaCu}_2\text{O}_8$ on bicrystalline substrates. *Physica C* 231, 123–129.
- Li, Q., Riley Jr, G.N., Parella, R.D., Fleshler, S., Rupich, M.W., Carter, W.L., Willis, J.O., Coulter, J.Y., Bingert, J.F., Parrell, J.A., Larbelestier, D.C., 1997. Progress in superconducting performance in rolled multifilamentary Bi-2223 HTS composite conductors. *IEEE Trans. Appl. Supercond.* 7, 2026–2029.
- Loane, R.F., Kirkland, E.J., Silcox, J., 1988. Visibility of single heavy atoms on thin crystalline silicon in simulated annular dark field STEM images. *Acta Cryst. A* 44, 912–927.
- Loane, R.F., Xu, P., Silcox, J., 1992. Incoherent imaging of zone axis crystals with ADF STEM. *Ultramicroscopy* 40, 121–138.
- Mannhart, J., Chaudhari, P., Dimos, D., Tsuei, C.C., McGuire, T.R., 1988. Critical currents in [001] grains and across their tilt boundaries in $\text{YBa}_2\text{Cu}_3\text{O}_7$ films. *Phys. Rev. Lett.* 61, 2476–2479.
- Mannhart, J., Hilgenkamp, H., 1998. Superconducting and normal state properties of $\text{YBa}_2\text{Cu}_3\text{O}_{7-\delta}$ bicrystal grain boundary junctions in thin films. *Appl. Phys. Letts.* 73, 265–267.
- Moeckly, B.H., Lathrop, D.K., Buhman, R.A., 1993. Electromigration study of oxygen disorder and grain-boundary effects in $\text{YBa}_2\text{Cu}_3\text{O}_{7-\delta}$ thin films. *Phys. Rev. B* 47, 400–417.
- Pashitskii, A.E., Polyanskii, A., Gurevich, A., Parrell, J.A., Larbelestier, D.C., 1995. Magnetic granularity, percolation, and preferential current flow in a silver-sheathed $\text{Bi}_{1.8}\text{Pb}_{0.4}\text{Sr}_2\text{Ca}_2\text{Cu}_3\text{O}_{8+x}$ tape. *Physica C* 246, 133–144.
- Pearson, D.H., Fultz, B., Ahn, C.C., 1988. Measurements of 3d state occupancy in transition metals using electron energy loss spectroscopy. *Appl. Phys. Letts.* 53, 1405–1407.
- Pennycook, S.J., Boatner, L.A., 1988. Chemically sensitive structure-imaging with a scanning transmission electron microscope. *Nature* 336, 565–567.
- Pennycook, S.J., Jesson, D.E., 1990. High resolution incoherent imaging of crystals. *Phys. Rev. Lett.* 64, 938–941.
- Pennycook, S.J., Jesson, D.E., 1991. High-resolution Z-contrast Imaging of Crystals. *Ultramicroscopy* 37, 14–38.
- Pennycook, S.J., Jesson, D.E., Browning, N.D., 1995. Atomic resolution electron energy loss spectroscopy in crystalline solids. *Nucl. Inst. Methods* 96, 575–582.
- Prouteau, C., Duscher, G., Browning, N.D., Pennycook, S.J., 1998. Investigation of the local superconducting properties in Ag-sheathed BSCCO tapes by STEM. *Physica C* 298, 1–9.
- Ravikumar, V., 1996 PhD Thesis, Northwestern University, USA.
- Sutton, A.P., Vitek, V., 1983. On the structure of tilt grain boundaries in cubic metals. 1. Symmetrical tilt boundaries. *Phil. Trans. R. Soc. Lond. A.* 309, 1–36.
- Sutton, A.P., 1988. Irrational tilt grain boundaries as one-dimensional quasicrystals. *Acta Metall.* 36, 1291–1299.
- Sutton, A.P., Balluffi, R.W., 1995. *Interfaces in Crystalline Materials*, Oxford University Press, Oxford.
- Wallis, D.J., Browning, N.D., 1997. Probing vacancies and structural distortions at ceramic grain boundaries with atomic resolution electron energy loss spectroscopy. *J. Am. Ceram. Soc.* 80, 781–785.
- Zhu, Y., Wang, Z.L., Suenaga, M., 1993. Grain boundary studies by the coincident site lattice model and electron energy loss spectroscopy of the oxygen K-edge in $\text{YBa}_2\text{Cu}_3\text{O}_{7-\delta}$. *Phil. Mag. A.* 67, 11–28.